# Photoinduced multimode coherent acoustic phonons of metallic nanoprisms and the effects of shape-induced anisotropic electronic stresses

Po-Tse Tai, Pyng Yu, and Jau Tang

Citation: The Journal of Chemical Physics **134**, 184506 (2011); doi: 10.1063/1.3590373
View online: http://dx.doi.org/10.1063/1.3590373
View Table of Contents: http://scitation.aip.org/content/aip/journal/jcp/134/18?ver=pdfcov
Published by the AIP Publishing

# Photoinduced multimode coherent acoustic phonons of metallic nanoprisms and the effects of shape-induced anisotropic electronic stresses

Po-Tse Tai,[1] Pyng Yu,[1] and Jau Tang[1,2,a)]
[1]*Research Center for Applied Sciences Academia Sinica, Taipei 11529, Taiwan*
[2]*Institute of Photonics, National Chiao-Tung University, Hsinchu 30010, Taiwan*

(Received 7 December 2010; accepted 25 April 2011; published online 11 May 2011)

In this work we reported experimental measurements of ultrafast structural dynamics in metallic nanoprisms induced by a femtosecond laser pulse. The main focus of this study of anisotropic heating in nanoprisms is about laser fluence effects on photoexcitation of two planar coherent acoustic phonon modes, namely, the breathing mode and the totally symmetric mode. We presented a combined two-temperature model and 2-D Fermi-Pasta-Ulam model to explain both the dependence of the initial phases and the mode weight on the excitation power. Our transient optical absorption data for both the initial fast monotonic decay and the subsequent coherent acoustic oscillations clearly indicate the presence of anisotropic thermal expansion in nanoprisms. © *2011 American Institute of Physics*. [doi:10.1063/1.3590373]

## I. INTRODUCTION

Recent development of nanofabrication techniques allows researchers to fabricate nanoparticles in various shapes and sizes. Because many physical properties of these nanoparticles strongly depend on their shapes and sizes, researchers could synthesize nanoparticles to achieve desired optical, electronic, thermal, or mechanical properties for specific applications.[1–7] To understand laser heating and laser processing of these nanomaterials it is important to investigate the thermo-mechanic properties via coherent phonon excitation using femtosecond laser pulses. Nanoparticles of various shapes and sizes have been widely investigated by optical pump-probe techniques and other techniques as well. The shapes of these nanoparticles include thin films, spheres, rods, prisms, disks, cubes, etc.[8–17]

Upon excitation by a femtosecond laser, the electrons in metals could be heated up suddenly to several thousands degrees. Although laser penetration depth is limited by the optical attenuation length, these hot electrons on the metal surfaces could move ballistically or diffusively much deeper inside the nanoparticles. Moreover, the fast thermal conduction of these electrons could quickly heat up colder electrons elsewhere to transfer their energies to the lattice. The sudden changes in the electron and phonon temperatures could induce impulsive thermal stresses[8,18,19] to cause the whole nanoparticles to vibrate. Because the optical refractive index, the absorption coefficient, and the surface reflectivity all depend on the particle sizes, one could use the optical transient absorption techniques to investigate such photoinduced coherent phonons. Comparing to the laser spot size, the nanoparticle is sufficiently small to experience almost uniform laser excitation. Therefore, one would expect an isotropic expansion in the nanoparticle. However, for nanoprisms, the apex is known to exhibit significant enhanced local field,[20,21] therefore, these sharp tips could possess stronger light absorption than elsewhere in a nanoprism. Consequently, we would expect a larger thermal gradient in a nanoprism to induce anisotropic thermal expansion even though these nanoparticles were under uniform light irradiation.

In order to treat anisotropic expansion of nanoprisms, we have employed the 2D Fermi-Pasta-Ulam (FPU) lattice model for a triangular-shaped atomic array to simulate planar lattice vibration. Although a nanoprism has a 3D structure in reality with its thickness as the third dimension, however, so long as its thickness is much smaller than the other two dimensions, our 2D simplification could capture the major relevant behavior. In our previous numerical simulation work,[22,23] a 2D FPU model with two types of impulsive forces was considered for nanoprisms to explain the origins of two planar phonon modes. These two modes include the breathing mode and the totally symmetric mode, where the vibration period of the first mode is related to the bisector of a triangular plane but the period of the second mode is related to half of the side length. Using this combined 2-D model we could nicely reproduce the experimentally observed dependence of the excitation power on the initial phase and the mode weight of these two phonon modes. We concluded that ballistic electron motion at a much higher laser excitation could cause a more uniform temperature distribution in the triangular plane and could lead to the suppression of the totally symmetric mode.

## II. SIMULATION MODEL

In a previous study,[9] we combined the 1D FPU model with the two-temperature model (TTM) to treat laser-heated metallic thin films. With TTM one could deal with the transient changes in the electron and phonon temperatures, and the resultant thermal stresses.[18,19] We consider here two types of impulsive forces that would capture the

a)Author to whom correspondence should be addressed. Electronic mail: jautang@gate.sinica.edu.tw.

 

major physical essence of TTM for the electron and phonon subsystems.[8,22–24] These two types of forces include the direct force corresponding to the change of the electron temperature and the indirect force corresponding to the change of the phonon temperature. Initially, upon heating by a laser pulse, the electrons are heated up to a very high temperature. Then, the energy is transferred to phonons via electron-phonon interactions. The rise of the electron temperature follows closely the rise of a femtosecond laser pulse but the drop of the electron temperature is dictated by the electron-phonon coupling time constant $\tau_{e\text{-}ph}$, which is on the order of a few picoseconds. Due to the heat transfer from the hot electrons, the rise of the phonon temperature occurs on a time constant of $\tau_{e\text{-}ph}$. At a much later time, the phonon temperature will eventually drop to the room temperature on a timescale of hundreds of picoseconds due to the relatively slow thermal dissipation to the heat bath.[25] Here, we consider two following types of forces, representing the temperature changes for the electron and phonon subsystems, respectively,

$$F_D = w_1 \times \exp\left(-\frac{t}{\tau_{e\text{-}ph}}\right) \times \exp\left(-\frac{z}{\lambda_1}\right),$$
$$F_I = w_2 \times \left[1 - \exp\left(-\frac{t}{\tau_{e\text{-}ph}}\right)\right] \times \exp\left(-\frac{z}{\lambda_2}\right), \quad (1)$$

where $F_D$ and $F_I$ represent the effective direct and indirect forces, $w_1$ and $w_2$ are the corresponding magnitudes, $z$ is the distance according to the direction of the temperature gradient, $\lambda_1$ and $\lambda_2$ are the corresponding penetration depths. Because the optical field directly heats up the electrons at the beginning, the initial hot electron distribution corresponds to the localized optical field. According to the previous studies,[20,21] the sharp tip exhibits an enhanced localized field, extending over several tens of nanometers. Thus, we would expect $\lambda_1$ to be on the same order of magnitude. Because of the ballistic motion and rapid thermal conduction, the initial hot electrons redistribute their energy among themselves, then transfer their energy to phonons. These phonons are not heated up directly by the heating laser pulse but by hot electrons.

A silver nanoprism is known to grow on the (111) plane of a fcc structure.[26,27] A triangular plane on the (111) plane is shown in Fig. 1. A spring is drawn between two adjacent atoms to represent the inter-atomic interaction. Because the force experienced by atoms in a metal is nondirectional, in our treatment each atom is assumed to sit in a spherical harmonic potential. In the FPU model, one could include an anharmonic term or even the Morse potential, however, because the amplitude of vibration is typically a few percentage of the bond length or smaller, the anharmonic effects could be neglected in this work. For nanoprisms, their apexes were known to enhance a strong localized field with a higher light absorption than the residual area.[20,21] Due to the polarization effects, for a randomly oriented nanoprism one tip orientation might be more parallel to the laser polarization than the others. For simplicity, we shall assume that the tip is along the z-axis. Because the tip has a much higher light absorption and it is more preferentially heated, therefore, the thermal gradient is along the bisector or z-axis. We consider here a 2D FPU model with

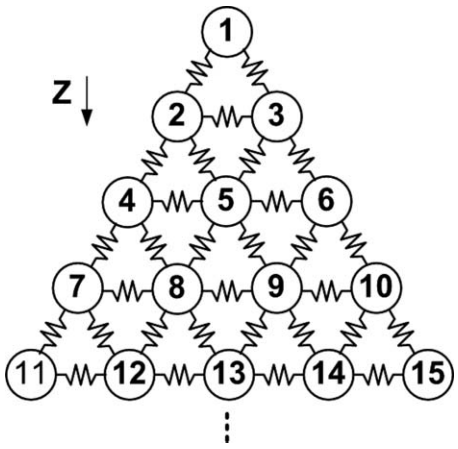


FIG. 1. A schematic diagram showing a triangular plate on the (1,1,1) plane of a fcc structure. In our simulation based on the FPU model, a 2D triangular atomic array with nearest neighbor coupling was used.

both direct and indirect forces taken into account to treat the ultrafast lattice dynamics of a triangular nanoplate, namely,

$$\frac{dS_n}{dt} = \frac{P_n}{m},$$
$$\frac{dP_1}{dt} = F_1 - \gamma P_1 - m\omega^2(S_1 - S_2) - m\omega^2(S_1 - S_3),$$
$$\frac{dP_2}{dt} = F_2 - \gamma P_2 - m\omega^2(S_2 - S_1) - m\omega^2(S_2 - S_3) - m\omega^2(S_2 - S_4) - m\omega^2(S_2 - S_5),$$
$$\vdots$$
$$\frac{dP_5}{dt} = F_5 - \gamma P_5 - m\omega^2(S_5 - S_2) - m\omega^2(S_5 - S_3) - m\omega^2(S_5 - S_4) - m\omega^2(S_5 - S_6) - m\omega^2(S_5 - S_8) - m\omega^2(S_5 - S_9),$$
$$\vdots \quad (2)$$

where $S_n$ is the atomic displacement in the z-axis for the $n$-th atom, $F_n$ is the impulsive force which consists of both direct and indirect forces due to thermally induced stresses caused by heated electrons and lattice, $P_n$ is the momentum, $\gamma$ is the damping factor, and $m\omega^2$ is the force constant. Following our previous studies,[22,23] we used $m\omega^2 = 14.29$ N/m for the silver nanoprism. The relationship between $F_I$ and $F_D$ will be discussed later in the Discussion section when we make a direct comparison between the simulation results with the experimental data. At time zero, the atoms are assumed to be at equilibrium position. Except for those atoms at the triangular boundary, each atom is connected to six adjacent atoms, and the equation of motion for each atom is described by Eq. (2). In our computer algorithm, we specially dealt with those boundary atoms, according to their specific couplings to adjacent atoms. We employed the Runge-Kutta method to numerically solve the above coupled equations.

## III. SIMULATED AND EXPERIMENTAL RESULTS

Before we proceed to discuss our simulation model, it is necessary to mention the magnitude relationship between $F_D$ and $F_I$. According to the previous studies,[8–10,22–24] the thermal stress $\sigma$ contains both lattice and electron contributions, It can be expressed as $\sigma = \sigma_e + \sigma_l = -\gamma_e C_e T_e \times \Delta T_e - \gamma_l C_l \times \Delta T_l$, where $\sigma_e$ and $\sigma_l$ are the stresses caused by hot electrons and lattice, or what we called direct and indirect forces in this paper, $C_l = 3.5 \times 10^6$ J m$^{-3}$ K$^{-1}$ and $C_e = 66$ J m$^{-3}$ K$^{-2}$ are the lattice and electron heat capacity, $\gamma_e = 0.97$ and $\gamma_l = 2.23$ are the Grüneisen parameters for electrons and lattice for silver, $T_e$ and $T_l$ are the electron and lattice temperatures, and $\Delta T_e$ and $\Delta_l$ are the electron and phonon temperature changes.[11,28] We utilized $\sigma_e$ and $\sigma_l$ to determine the magnitude for $F_D$ and $F_I$. Based on the two-temperature model, the maximum electron temperature could be estimated from $\tau_{e\text{-}ph} \times g/C_e$,[11] where the electron-phonon coupling constant $g = 3 \times 10^{16}$ W m$^{-3}$ K$^{-1}$.[11,17] We can obtain the value for $\tau_{e\text{-}ph}$ from the experiment, which depends on the excitation power. Taking our experimental results as an example, the transient absorption result at an excitation power of 0.5 $\mu$J/pulse allowed us to determine $\tau_{e\text{-}ph} = 3.8$ ps, which could then be substituted into the formula to obtain an estimate of the maximum electronic temperature of 1727 K while the initial temperature is 300 K. With complete electron-phonon thermalization, we could obtain the maximum temperature for the lattice to be 346 K. The ratio of the force magnitudes between $F_I$ and $F_D$ is $w_1/w_2 = 0.435$. Therefore, we could determine $\tau_{e\text{-}ph}$ from the experimental results and then calculate the relative magnitude between $F_D$ and $F_I$ of the simulation model. This procedure allows us to relate the lattice vibration with the excitation power.

Using our 2D model for nanoprisms we determined two planar phonon modes, the breathing mode and the totally symmetric mode.[22,23] In model simulations, we considered a triangular plane similar to the size used in the experiments, which has a 43 nm bisector containing 14 112 atoms. From the fits to the experimental results, we obtained $\lambda_1 = 20$ nm and $\lambda_2 = 160$ nm. The parameter $\tau_{e\text{-}ph}$, which depends on the excitation power, was determined from the transient absorption, results for us to estimate the force magnitude. We presented the dependence of the initial phase on $\tau_{e\text{-}ph}$ in Fig. 2(a), where the open squares and open circles represent the simulated results of the breathing mode and the totally symmetric mode, respectively. It is clearly shown that the initial phases of the breathing mode and the totally symmetric mode both decrease as $\tau_{e\text{-}ph}$ increases, except that for the breathing mode the decreases are more rapid. The phase difference between both modes drops from 110° to 45° as $\tau_{e\text{-}ph}$ increases.

Here, we will discuss the relative amplitude of each mode. The mode weight of the totally symmetric mode is defined as the amplitude ratio between the totally symmetric mode and the breathing mode. The open circles shown in Fig. 2(b) represent the simulated results. It is obvious that the mode weight decreases as $\tau_{e\text{-}ph}$ increases. From the previous study,[13,22,23] the excitation of the totally symmetric mode is attributed to the ballistic electron stress, or $F_D$. As the excitation power increases, $F_D$ becomes more dominant and the ratio of $w_1/w_2$ increases. However, a dominating $F_D$ implies an opposite trend for the mode weight in Fig. 2(b). The breathing modes excited by either $F_D$ or $F_I$ are nearly out of phase. This phase mismatching would cause destructive interference in the oscillatory pattern for the breathing mode with excitation by both $F_D$ and $F_I$. Therefore, due to destructive interference for the breathing mode, the relatively weak, totally symmetric mode becomes more prominent to stand out.[22,23] Consequently, the mode weight of the totally symmetric mode could become more dominant depending on the extent of destructive interference. The above reasoning offers a sound explanation to why that the mode weight decreases as $\tau_{e\text{-}ph}$ increases.

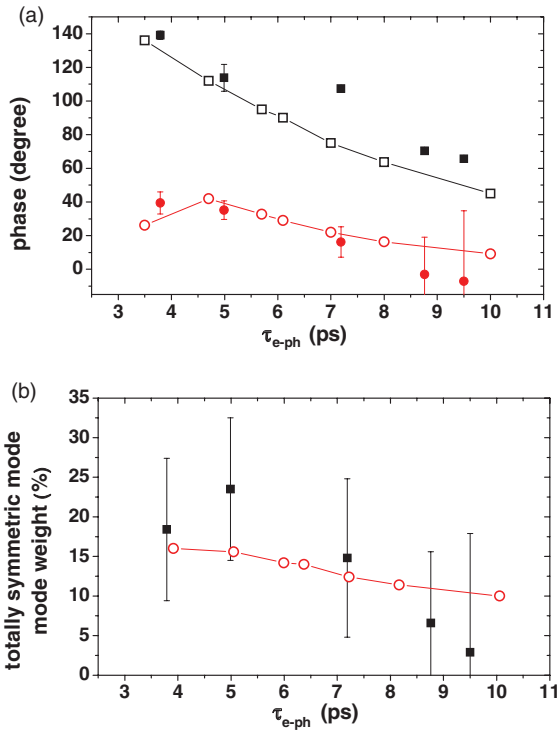


FIG. 2. (a) Initial phase dependence on the electron-phonon coupling time. We arranged the simulated data curves with open squares to represent the breathing mode, and open circles to represent the totally symmetric mode, in comparison with solid spots from the experimental measurements. (b) The dependence of the mode weight of the totally symmetric mode on the electron-phonon coupling time. The mode weight of the totally symmetric mode is defined as the ratio between the amplitude of the totally symmetric mode and that of the breathing mode. The open circles and solid circles represent the numerical and experimental results, respectively.

The silver nanoprisms were prepared by a chemical synthesis method described previously.[17,29] The dimension of the resulting silver nanoprisms with ~43 nm bisector and ~7 nm thickness was determined from images taken by TEM. The histogram of the bisectors is shown in the inset of Fig. 3(a). The UV-visible extinction spectrum of nanoprisms is shown in Fig. 3(b) and the vertical dashed line represents the wavelength of the pump and probe beam. Different from the report by Chergui *et al.*,[13] we were able to observe in this work the totally symmetric mode around the SPR peak, and this observation is consistent with our previous study about optical control of coherent acoustic vibrations.[29]

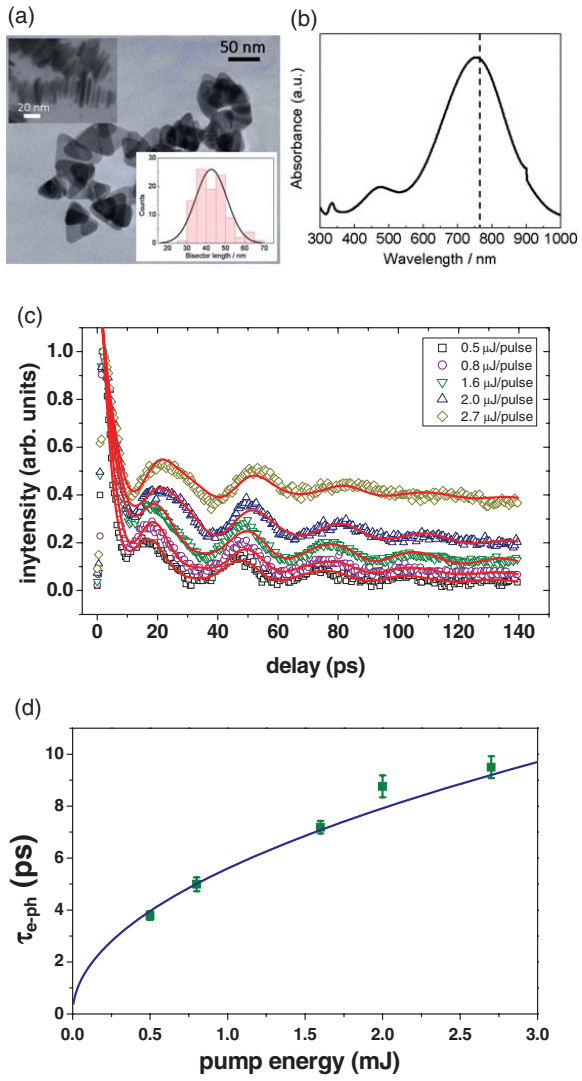


FIG. 3. (a) TEM image of the silver nanoprisms. Inset is the size distribution of the bisector length of the silver nanoprisms. (b) UV-visible spectra of the silver nanoprisms. The dashed line is the wavelength of the pump and probe beams. (c) The observed transient absorption profiles with a different pump power. The red lines are the results of the global fit by Eq. (3). (d) The dependence of the electron-phonon coupling constant on the excitation laser energy. The blue curve represents the best fit to the experimental data.

A transient absorption setup was employed to investigate the coherent phonons of nanoprisms. Laser pulses of 100 fs with 1 KHz repetition rate were provided from the regenerative amplifier. The femtosecond pulses were split into the pump and probe beam with the pump/probe energy ratio of 100 to 1. The probed beam was detected by a photodiode detector, and the variant transmittance dependence on time delay was acquired by a personal computer through a lock-in amplifier. The perpendicular polarization between the pump and probe beams was chosen to minimize the scattered light from the pump beam. During the measurement time, the sample was circulated in a flow cell with 1 mm optical path.

The transient absorption data curves for silver nanoprisms are shown in Fig. 3(c) from the measurements under different excitation powers. The large peak that occurs before 10 ps is due to photoinduced hot-electron dynamics, and the subsequent damped sinusoidal oscillations are due to coherent acoustic phonons. Our experimental data curves were fitted by the following equation, similar to Chergui's work:[13]

$$A_e \exp\left(-\frac{t}{\tau_{e\text{-}ph}}\right) + A_{br}\cos\left(\frac{2\pi t}{\tau_{br}} + \phi_{br}\right)\exp\left(-\frac{t}{\tau_{dbr}}\right) + A_{to}\cos\left(\frac{2\pi t}{\tau_{to}} + \phi_{to}\right)\exp\left(-\frac{t}{\tau_{dto}}\right) + A\exp\left(-\frac{t}{\tau_1}\right), \quad (3)$$

Several parameters were used in the above equation, including the electron-phonon coupling time constant $\tau_{e\text{-}ph}$, thermal dissipation decay time $\tau$, periods, and phases for two damped oscillations. The oscillation periods were determined from the fitting with $\tau_{br} = 29.4$ ps for the breathing mode and $\tau_{to} = 18.1$ ps for the totally symmetric mode. The period of the coherent acoustic oscillations could be approximated by $2L/v_s$, where $v_s$ is the sound velocity, 3650 m/s, and $L$ is related to the nanoparticle size. The breathing mode is related to the bisector height and the totally symmetric mode is related to half of the edge length.[13,14,22,23,29] The underestimate of the size using the above approximate relation was noted in previous studies using a variational approach to solve the elastodynamics problem.[13,14]

Shown in Fig. 2(a) is the dependence of the initial phase of the breathing mode $\phi_{br}$ and the totally symmetric mode $\phi_{to}$ on $\tau_{e\text{-}ph}$, represented by the solid squares and circles, respectively. Using the simulation model, we could nicely reproduce the experimental results. The mode weight of the totally symmetric mode $A_{to}/A_{br}$ is shown in Fig. 2(b). Comparing to the simulation results, the mode weight rapidly decreases as $\tau_{e\text{-}ph}$ exceeds 8 ps. The fitted results agree with our previous observation of optical control of coherent acoustic vibrations.[29] Because the totally symmetric mode is relatively small at a higher excitation power, the error bar of $\phi_b$ shown in Fig. 2(a) is slightly larger.

In a regime at a relatively low electron temperature, TTM is a useful tool to deal with the condition of the electron-phonon nonequilibrium. As the electron temperature becomes sufficiently higher, above 5000 K for silver,[30] the electron heat capacity $C_e$ and the electron-phonon coupling constant $g$ becomes to depend more strongly on the electron temperature. The formula of $\tau_{e\text{-}ph} \times g/C_e$, which we used in this work, could cause an overestimate of the maximum electron temperature. The electron temperature would approach 5000 K when $\tau_{e\text{-}ph} = 10$ ps. In order for the estimation formula to be valid, $\tau_{e\text{-}ph}$ should be below 10 ps. In Fig. 3(d), we rearranged $\tau_{e\text{-}ph}$ which was determined from the experimentally observed pump power dependence. The maximum $\tau_{e\text{-}ph}$ was found to be below 10 ps. When the electron temperature reaches the maximum, it is reasonable to assume that the energy comes from the heating laser pulse because the coupling to the phonons occurs much later. Based on the energy conservation, one has $\int_{300}^{T_{emax}} C_e T_e \times l^3 dT_e = P \times a$, where $T_{e\,max}$ is the maximum electron temperature, $P$ is the pump laser energy, $a$ is the aborted fraction of the laser beam, $l$ is the bond distance, and 300 is the initial electron temperature. The relationship between the maximum electron temperature and the

pump energy could be expressed by

$$T_{e\max} = \sqrt{\frac{2 \times P \times a}{C_e \times l^3} + 300^2}. \quad (4)$$

We combined Eq. (4) with the simplified formula of $T_{e\max} = \tau_{e-ph} \times g/C_e$ derived from TTM, for experimental data fitting. The blue curve represents the fitted result. From the previous study,[11] the intercept could be used to estimate the electron-phonon coupling constant. A reasonable intercept value of 600 fs was obtained from the fit.[11] Furthermore, in Fig. 3(d), the electron-phonon coupling time follows the prediction of TTM. It means that the simplified estimation formula based on TTM was a valid approximation in our experimental conditions.

At a higher excitation power, the mode weight in Fig. 2(b) was found to rapidly decrease with a large deviation from the simulation results. The tips of nanoprisms were found experimentally to be truncated due to higher laser irradiation.[18,31] Unlike the ideal sharp tips, the snipped tips could cause a decrease in the optical absorption and a more uniform initial distribution of the electron temperature. Since the SPR peak is sensitive to snipping,[18,31] we could use the absorption spectrum to estimate the extent of snipped nanoprisms. After transient absorption experiment, we found that the peak of SPR is blue-shifted by about 10 nm, indicating that the nanoprisms were snipped slightly.[20] The results in Fig. 3 from the transient absorption experiments also support this analysis. The period of the breathing mode should depend on the particle sizes, but the period did not change under the maximum excitation. The tips, which were snipped slightly, could enhance the localized optical field to cause anisotropic electron stresses on the triangular plane. For sniped nanoprisms, we neglected the effects on the mode weight of the totally symmetric mode. From the viewpoint of model simulation, the mode weight of the totally symmetric mode should be strongly related to $\lambda_1$, the force penetration depth of $F_D$, the stationary excitation power, and $\tau_{e\text{-}ph}$. With a larger $\lambda_1$ the electron thermal distribution is more uniform, and it would result in a significant decrease in the totally symmetric mode weight. To have a better agreement with the experimental results, a larger $\lambda_1$ should be used which certainly depends on the excitation power. This parameter $\lambda_1$ depends on the optical field distribution on the triangular plane or the initial hot electron distribution. The ballistic motion of hot electrons could quickly transfer heat to adjacent areas to cause a more uniform electron temperature distribution. We could attribute the deviation between the experiments and the simulation to more efficient heat transfer via ballistic motion under higher laser excitation.

## IV. CONCLUSIONS

In this study of silver nanoprisms by transient optical absorption techniques, we investigated the effects of excitation intensities on the short-time monotonous decay of the data and the initial phase of the subsequent oscillatory acoustic vibrations. Moreover, we presented here a simulation model to explain and to quantify the experimentally observed dependence of the electron-phonon coupling time constant and the phase of the acoustic oscillations. According to this model that is based on the notion of an enhanced optical field localized near the sharp tips of a nanoprism, we theorized that the geometrical distribution of thermal gradient on the triangular plate was the source for causing anisotropic thermal expansion. Two planar coherent acoustic modes, namely, the breathing mode and the totally symmetric mode, were directly observed, as inferred by this anisotropic expansion model. Furthermore, we applied this model to analyze the influences of the excitation power on the initial phase and the mode weight of two such planar phonon modes. In addition, we observed that when the excitation power exceeded a threshold, the mode weight of the totally symmetric mode is rapidly decreased. This behavior could be attributed to fast electron ballistic motion which would cause a more uniform thermal distribution, i.e., a smaller thermal gradient. Therefore, the totally symmetric mode would become more suppressed.

## ACKNOWLEDGMENTS

J.T. thanks the support of the Academia Sinica and National Science Council (NSC) of Taiwan under the Program Nos. 98–2221-E-001–019 and 99–2221-E-001–002-MY3. P.T.T. and P.Y. acknowledge NSC and Academia Sinica for providing postdoctoral fellowship, respectively.

[1] V. I. Klimov, J. Phys. Chem. B **110**, 16827 (2006).
[2] D. E. Chang, A. S. Sorensen, E. A. Demler, and M. D. Lukin, Nat. Phys. **3**, 807 (2007).
[3] K. Kneipp, H. E. H Kneipp, I. Itzkan, R. R. Dasari, and M. S. Feld, J. Phys. Condens. Matter **14**, 597 (2002).
[4] J. R. Krenn, Nature Mater. **2**, 210 (2003).
[5] A. V. Kabashin, P. Evans, S. Pastkovsky, W. Hendren, G. A. Wurtz, R. Atkinson, R. Pollard, V. A. Podolskiy, and A. V. Zayats, Nature Mater. **8**, 867 (2009).
[6] W. L. Barnes, A. Dereux, and T. W. Ebbesen, Nature (London) **424**, 824 (2003).
[7] C. T. Yuan, P. Yu, and J. Tang, Appl. Phys. Lett. **94**, 243108 (2009).
[8] P. T. Tai, P. Yu, and J. Tang, J. Phys. Chem. C **113**, 15014 (2009).
[9] J. Tang, D. S. Yang, and A. H. Zewail, J. Phys. Chem. C **111** , 8957 (2007).
[10] M. Perner, S. Gresillon, J. Marz, G. Von Plessen, J. Feldmann, J. Porstendorfer, K. J. Berg, and G. Berg, Phys. Rev. Lett. **85**, 792 (2000).
[11] J. H. Hodak, A. Henglein, and G. V. Hartland, J. Chem. Phys. **111**, 8613 (1999).
[12] G. V. Hartland, Phys. Chem. Chem. Phys. **6**, 5263 (2004).
[13] L. Bonacina, A. Callegari, C. Bonati, F. Van Mourik, and M. Chergui, Nano Lett. **6**, 7 (2006).
[14] J. Burgin, P. Langot, N. D. Fatti, F. Vallee, W. Huang, and M. A. El-Sayed, J. Phys. Chem. C **112**, 11231 (2008).
[15] A. Crut, P. Maioli, N. D. Fatti, and F. Vallee, Phys. Chem. Chem. Phys. **11**, 5882 (2009).
[16] H. Petrova, C. H. Lin, S. de Liejer, M. Hu, J. M. McLellan, A. R. Siekkinen, B. J. Wiley, M. Marquez, Y. Xia, J. E. Sader, and G. V. Hartland, J. Chem. Phys. **126**, 094709 (2007).
[17] P. Yu, J. Tang, and S. H. Lin, J. Phys. Chem. C **112**, 17133 (2008).
[18] O. B. Wright, Phys. Rev. B **49**, 9985 (1994).
[19] J. K. Chen, J. E. Beraun, L. E. Grimes, and D. Y. Tzou, Int. J. Solids Struct. **39**, 3199 (2002).
[20] K. L. Kelly, E. Coronado, L. L. Zhao, and G. C. Schatz, J. Phys. Chem. B **107**, 668 (2003).
[21] L. Novotny, R. X. Bian, and X. S. Xie, Phys. Rev. Lett. **79**, 645 (1997).
[22] P. T. Tai and J. Tang, J. Sci. Conf. Proc. **1**, 207 (2009).
[23] P. T. Tai, P. Yu, and J. Tang, Chem. Phys. **374**, 126 (2010).
[24] C. Voisin, N. D. Fatti, D. Christofilos, and F. Vallee, Appl. Surf. Sci. **164**, 131 (2000).

[25]J. H. Hodak, I. Martini, and G. V. Hartland, J. Phys. Chem. B **102**, 6958 (1998).
[26]B. Rodríguez-González, I. Pastoriza-Santos, and L. M. Liz-Marzán, J. Phys. Chem. B **110**, 11796 (2006).
[27]K. J. Bikash and R. C. Retna, J. Phys. Chem. C **111**, 15146 (2007).
[28]T. H. K. Barron, J. G. Collins, and G. K. White, Adv. Phys. **29**, 609 (1980).
[29]P. T. Tai, P. Yu, and J. Tang, Chem. Phys. Lett. **496**, 326 (2010).
[30]Z. Lin and L. V. Zhigilei, Phys. Rev. B **77**, 075133 (2008).
[31]Q. Zhang, J. Ge, T. Pham, J. Goebl, Y. Hu, Z. Lu, and Y. Yin, Angew. Chem., Int. Ed. **48**, 3516 (2009).